Sulfasalazine-induced ferroptosis in breast cancer cells is reduced by the inhibitory effect of estrogen receptor on the transferrin receptor

HAOCHEN YU[1,2*], CHENGCHENG YANG[3*], LEI JIAN[1,2], SHIPENG GUO[1,2], RUI CHEN[1],
KANG LI[1], FANLI QU[1], KAI TAO[4], YONG FU[5], FENG LUO[1] and SHENGCHUN LIU[1]

[1]Department of Endocrine and Breast Surgery, The First Affiliated Hospital of Chongqing Medical University,
Chongqing 400016; [2]Chongqing City Key Lab of Translational Medical Research in Cognitive Development and Disorders,
Children's Hospital of Chongqing Medical University, Chongqing 400014; [3]Department of Breast Surgery,
The People's Hospital of Deyang, Deyang, Sichuan 618000; [4]Department of The Second of Gynecologic Oncology,
Shaanxi Provincial Tumor Hospital, The Affiliated Hospital of Medical College of Xi'an JiaoTong University,
Xi'an, Shaanxi 710061; [5]Department of Breast Surgery, Dianjiang People's Hospital of Chongqing,
Dianjiang, Chongqing 408300, P.R. China

Abstract. The aim of the present study was to clarify the activation of ferroptosis in different breast cancer cells by sulfasalazine (SAS) and to explore the relationship between the estrogen receptor (ER) and the transferrin receptor (TFRC). MDA-MB-231 and T47D cells were treated with SAS for 24 h. Changes in cell morphology were observed under a microscope. CCK-8 was used to detect the proliferation inhibition rate and determine the IC_{50} values. Western blotting was used to detect the expression of glutathione peroxidase 4 (GPX4) and xCT. Flow cytometry was used to identify changes in the production of reactive oxygen species (ROS). Mitochondrial morphological changes in T47D were observed using transmission electron microscopy. Changes in the mitochondrial membrane potential (MMP) were observed using confocal fluorescence microscopy. RT-PCR was used to detect the mRNA expression levels of TFRC and divalent metal transporter 1 (DMT1). Bioinformatics analysis was performed on TFRC expression in 1,208 breast cancer samples and its relationship with ER. TFRC expression was detected in various breast cancer tissues using immunohistochemistry and in various breast cancer cells using western blotting. Small interfering RNA (siRNA) knocked down ER expression in T47D cells, and changes in the TFRC mRNA and protein levels were observed. RT-PCR was used to detect TFRC expression in 87 clinical specimens. The results of the present study revealed that SAS could inhibit breast cancer cell viability, which was accompanied by an abnormal increase in ROS and a depletion of GPX4 and system x_c^-. Liproxstatin-1 reversed the SAS-induced increase in ROS. The cells treated with SAS had shrunken mitochondria and decreased MMP. SAS upregulated TFRC and DMT1. Knockdown of the ER increased TFRC expression in breast cancer cells. Immunohistochemistry indicated that TFRC expression was lower in ER^+ tissues than in ER^- tissues. After confirmation with RT-PCR in 87 clinical specimens, TFRC expression in ER^- tissue was revealed to be significantly higher than that of ER^+ tissue. In conclusion SAS could trigger ferroptosis in breast cancer cells, especially in cells with low ER expression. Therefore, SAS is a potential agent for breast cancer treatment.

Correspondence to: Dr Shengchun Liu or Professor Feng Luo, Department of Endocrine and Breast Surgery, The First Affiliated Hospital of Chongqing Medical University, 1 Youyi Road, Yuanjiagang, Yuzhong, Chongqing 400016, P.R. China
E-mail: luofeng@hospital.cqmu.edu.cn
E-mail: liushengchun@hospital.cqmu.edu.cn

*Contributed equally

Introduction

Breast cancer is the most common form of cancer and the leading cause of cancer-related deaths among females worldwide (1). The development of breast cancer therapies is expensive and slow. Additionally, substantial heterogeneity exists within and between well-established breast cancer subtypes and drug responses (2). Three distinct features can be used to group breast tumors based on the following: Morphological criteria (e.g., ductal, lobular, invasive and *in situ*); expression of the estrogen receptor (ER), progesterone receptor (PR), and Her2 receptor tyrosine kinase (Her2); or molecular phenotypes, based on comprehensive mRNA similarities (e.g., luminal and basal). Approximately one-fourth of breast tumors are

'triple-negative' [ER$^-$/PR$^-$/Her2$^-$; triple-negative breast cancer (TNBC)] and usually have a basal molecular phenotype. Due to chemotherapy resistance and the lack of TNBC-targeted therapeutics, patient prognosis is grim. Conversely, 20% of breast cancer patients suffer from Her2$^+$ breast cancer. This patient population requires expensive targeted therapy. Therefore, effective breast cancer treatments are desired by doctors and patients.

Ferroptosis is a recently recognized form of regulated cell death. It is morphologically characterized by the presence of mitochondria that are smaller than normal in size. Ferroptosis can be induced by experimental compounds (e.g., erastin) or clinical drugs (e.g., sorafenib and artemisinin) in cancer cells and certain normal cells (e.g., kidney tubule cells, fibroblasts and T cells) (3-5). Ferroptosis is characterized by the accumulation of lipid peroxidation products and toxic reactive oxygen species (ROS) derived from iron metabolism and can be pharmacologically inhibited by iron chelators (e.g., deferoxamine) and lipid peroxidation inhibitors (e.g., ferrostatin-1 and liproxstatin-1) (5,6). Iron metabolism and lipid peroxidation signaling are increasingly being recognized as central mediators of ferroptosis (7). The inhibition of cystine/glutamate antiporters (system x$_c^-$) and increasing accumulation of iron are involved in the induction of ferroptosis (5). xCT is a functional subunit of system x$_c^-$ that regulates the exchange of glutamate and cystine in cells. xCT is a light chain encoded by the SLC7A11 gene that comprises system x$_c^-$, and thus, xCT expression can be used as a surrogate of system x$_c^-$ expression (8).

Sulfasalazine (SAS) is broadly used to treat chronic inflammation in the gut, joints, and retina. In addition to inhibiting the NF-κB signaling pathway, SAS inhibits the system x$_c^-$ transporter (9). Given that the disruption of system x$_c^-$-mediated cystine uptake by erastin is sufficient to induce ferroptosis, treatment of cancer cells (e.g., HT1080) with SAS can also trigger ferroptosis (10). However, the effect of SAS on iron metabolic pathways in ferroptosis is not clear. Previous studies have revealed that SAS can induce ferroptosis in pancreatic cancer cells, and thus, ferroptosis may be a new option for treating pancreatic cancer (11). Nevertheless, whether SAS can induce ferroptosis in different breast cancer cells has not been clearly reported.

Investigations on this topic may confirm whether SAS can induce ferroptosis in different breast cancer cells and lead to an improved molecular understanding of how SAS induces ferroptosis, especially the relationship of SAS with iron metabolism. ER expression is an important basis of breast cancer molecular phenotyping. Transferrin receptor (TFRC) is a key factor in iron metabolism (12). When exploring the relationship between ER and TFRC, it was revealed that ER can inhibit TFRC expression. Since ER is differentially expressed in various breast cancer subtypes, it is possible that this inhibition can lead to differences in the sensitivity of breast cancer cells to SAS-induced ferroptosis. Therefore, a novel relationship between ER and TFRC in the regulation of ferroptosis with important information regarding SAS-mediated anticancer therapy is presented. The purpose of the present study was to determine whether SAS can induce ferroptosis in breast cancer cells. It was hypothesized that breast cancer cells have different sensitivities to SAS since the different expression

levels of ER in breast cancer cells have different inhibitory effects on TFRC.

Materials and methods

Cell culture. MDA-MB-231, T47D, BT549 and MCF7 human breast cancer cells were purchased from the American Type Culture Collection (ATCC) and grown in medium supplemented with 10% heat-inactivated fetal bovine serum (HI-FBS), 100 μg/ml streptomycin, and 100 units/ml penicillin (Invitrogen; Thermo Fisher Scientific, Inc.) in a humidified incubator with 5% CO_2 at 37°C.

Detection of ROS. The intracellular ROS level in the form of cellular peroxides was assessed using a Reactive Oxygen Species Assay Kit (Beyotime Institute of Biotechnology) after treatment with or without SAS (Abcam) and liproxstatin-1 (MedChemExpress). In the liproxstatin-1-treatment group, the cells were treated with 300 nM liproxstatin-1 for 24 h before the addition of SAS. The cells were collected, exposed to 10 μM 2',7'-dichlorofluorescein diacetate (DCFH-DA), and incubated at 37°C for 20 min. The cells were washed three times with PBS, and fluorescence intensity was analyzed by flow cytometry (excitation at 488 nm; emission at 525 nm). ROS levels were expressed as the mean fluorescence intensity of 20,000 cells. Three independent experiments were performed.

RNA isolation and real-time PCR (RT-PCR). Total RNA from MDA-MB-231 and T47D cells was extracted with a total RNA extraction kit and reverse-transcribed using the PrimeScript RT reagent kit (Promega Corporation). Quantitative RT-PCR was performed using SYBR Premix Ex Taq^{TM} II (Takara Bio, Inc.) in a 10-μl PCR mixture on a Bio-Rad CFX96 Real-Time PCR system (Bio-Rad Laboratories, Inc.) according to the manufacturer's standard protocols. An initial cycling for 2 min at 95°C, followed by 39 cycles at 95°C for 30 sec, 30 sec at 58°C and 20 sec at 72°C. The primer sequences were as follows: Divalent metaltransporter 1 (DMT1) forward, 5'-AGCTCCACCATGACAGGAACCT-3' and reverse, 5'-TGGCAATAGAGCGAGTCAGAACC-3'; TFRC forward, 5'-ATCGGTTGGTGCCACTGAATGG-3' and reverse, 5'-ACAACAGTGGGCTGGCAGAAAC-3'; glyceraldehyde 3-phosphate dehydrogenase (GAPDH) forward, 5'-TGACTTCAACAGCGACACCCA-3' and reverse, 5'-CACCCTGTTGCTGTAGCCAAA-3'; and estrogen receptor 1 (ESR1) forward, 5'-GGTCAGTGCCTTGTTGGATG-3' and reverse, 5'-CAGGTTGGTGAGTAAGC-3'. Three independent experiments were performed for each group. Relative gene expression was normalized to GAPDH and calculated using the $2^{-\Delta\Delta Cq}$ method (13).

Cell viability assay. Cell growth and SAS-mediated inhibition were detected using the Cell Counting Kit-8 (CCK-8; Beyotime Institute of Biotechnology). According to the manufacturer's instructions, cells were plated at a density of 2.5×10^4/well in 96-well plates with or without different concentrations of SAS, and cell viability was assessed at 24 h. The absorbance of each well was measured at a wavelength of 450 nm using a Synergy H1 microplate reader (BioTek Instruments, Inc.). Empty wells served as blank controls. The test was performed three times under the same operating conditions. The cells were treated with

SAS at concentrations of 0.1, 0.5, 1.0, 1.5, 2.0, and 3.0 mM, and cell viability was determined using the CCK-8 assay at 24 h. The half maximal inhibitory concentration (IC_{50}) of SAS for different cells was calculated according to the standard curve.

Western blot analysis. Cell were washed twice with cold PBS and harvested. Protein lysates were prepared from MDA-MB-231 and T47D cells using a protein extraction kit (Nanjing KeyGen Biotech. Co. Ltd.). Protein concentrations were assessed using a BCA Protein Assay kit (Beyotime Institute of Biotechnology). Equal amounts of proteins (40 μg/lane) from each group were separated by sodium dodecyl sulfate polyacrylamide gel electrophoresis on 12.5% gels (Bio-Rad Laboratories, Inc.) and transferred to polyvinylidene difluoride membranes (EMD Millipore). After blocking with 5% skim milk for 1 h at room temperature, the membranes were incubated with specific primary antibodies at 4˚C overnight. Then, after washing three times with Tris-buffered saline containing Tween-20, the membranes were incubated with horseradish peroxidase-conjugated secondary antibodies for 1 h at room temperature. Proteins were visualized by chemiluminescence using enhanced chemiluminescent substrate (Beyotime Institute of Biotechnology). Immunoreactive bands were examined using the ChemiDoc Imaging System (Bio-Rad Laboratories, Inc.). The following antibodies were used: Rabbit anti-xCT antibody (cat. no. 12691S; dilution 1:800; Cell Signaling Technology, Inc.); rabbit anti-glutathione peroxidase 4 (GPX4) antibody (cat. no. SAB2108670; dilution 1:1,000; Sigma-Aldrich; Merck KGaA); rabbit anti-ESR1 (cat. no. 13258; dilution 1:1,000) and rabbit anti-TFRC (cat. no. 13113; dilution 1:1,000; both from Cell Signaling Technology, Inc.); and rabbit anti-GAPDH (cat. no. ATGA0181; dilution 1:1,000; 4A Biotech Co., Ltd.). Horseradish peroxidase-conjugated goat anti-rabbit antibodies were used as secondary antibodies (cat. no. 7074S; dilution 1:1,000; Cell Signaling Technology, Inc.). GAPDH was used as an internal control for each membrane.

Electron microscopy. After the indicated treatment, cells on a 100-mm dish were fixed in 2.5% glutaraldehyde in 0.1 M PBS (pH 7.4) at room temperature for 1 h, post-fixed in 1% OsO_4 in 0.1 M PBS (pH 7.4) at room temperature for 1 h, dehydrated using a graded series of ethanol and embedded with epoxy resin and sectioned. Ultrathin (60-nm) sections were collected on grids and stained with uranyl acetate and lead citrate. Images were obtained using an H-7100 transmission electron microscope (Hitachi, Ltd.).

siRNA transfection assay. Cells were plated in six-well plates and transfected with specific siRNAs using Lipofectamine™ 2000 transfection reagent (Invitrogen; Thermo Fisher Scientific, Inc.) according to the manufacturer's instructions. Two siRNA sequences were used to ensure the accuracy of the experiment. The sequences of siRNA were as follows: ESR1-siRNA1 (sense 5'-GGAGGAUGUUGAAACACA ATT-3', antisense 5'-UUGUGUUUCAACAUUCUCCTT-3') and ESR1-siRNA2 (sense 5'-GGAUUUGACCCUCCA UGAUTT-3', antisense 5'-AUCAUGGAGGGUCAAAUC CTT-3'). All siRNA oligomers were purchased from Shanghai GenePharma Co., Ltd.

Immunohistochemistry (IHC). The human tissues were fixed with 4% formaldehyde buffer, the fixed time of the specimens was 12-24 h at room temperature 15-28˚C. Deparaffinized specimens were then sectioned at 4-μm-thick slices. The slices were autoclaved at 115˚C for 5 min for antigen retrieval in citric acid buffer (pH 6.0) and quenched for endogenous peroxidase activity with 0.3% H_2O_2 solution for 10-15 min. Then, the samples were blocked for nonspecific binding with normal goat serum for 10-15 min and incubated with the specific rabbit primary antibody against TFRC (cat. no. PB9233; dilution 1:700; Boster Biological Technology Co., Ltd.) overnight at 4˚C. Subsequently, the sections were treated with the goat anti-rabbit antibody for 30 min at room temperature. After staining with diaminobenzidine (DAB) (cat. no. PV-9000; Beijing Zhongshan Golden Bridge Biotechnology Co., Ltd.; OriGene Technologies), images were captured using a Nikon Eclipse 80i microscope (Nikon Corporation).

Mitochondrial membrane potential assay. The mitochondrial membrane potential (MMP) was assayed using tetramethylrhodamine methyl ester (TMRM) according to the manufacturer's instructions (AAT Bioquest, Inc.). TMRM is readily sequestered by healthy mitochondria, but its fluorescence is rapidly lost when the MMP dissipates. Cells were seeded in confocal dishes before treatment with or without SAS. The cells were washed twice with PBS and incubated for 20 min at 37˚C with 100 nM TMRM for staining mitochondria and then carefully washed three times with PBS. To ensure the accuracy of MMP detection, cell activity should be maintained when staining for TMRM; the cells should not be killed by reagents such as formaldehyde. Finally, the cells were analyzed by confocal fluorescence microscopy (Nikon N-SIM; Nikon Corporation) to assess the intensity of red fluorescence (excitation at 549 nm; emission at 573 nm).

Collection of clinical tissue samples and RNA extraction. In the present study, clinical tissue samples were collected from 87 patients with breast cancer, and RNA was extracted. The human breast cancer specimens used in this study were collected in the operating room of the Department of Endocrine and Breast Surgery, First Affiliated Hospital of Chongqing Medical University, from July 2015 to June 2017. All clinical specimens were diagnosed by clinical and pathological examinations, and all patient information data were true and valid. The First Affiliated Hospital of Chongqing Medical University Ethics Committee reviewed and approved the use of human tissue specimens and all patients provided written informed consent. Additional information for these patients is provided in Table I. RNA from the tissue samples from 87 patients was extracted with a total RNA extraction kit and reverse-transcribed using the PrimeScript RT reagent kit (Promega Corp.).

Bioinformatics analysis. Data was downloaded from The Cancer Genome Atlas (TCGA) database (https://cancergenome.nih.gov) for 1,208 breast cancer samples. TFRC expression was analyzed in different subtypes of breast cancer cells and the correlation between TFRC and ESR1 with ggstatspot (a package in R, version 3.5.1). TFRC expression in cancer tissues and normal tissues was determined using Gene

Table I. Characteristics of all patients (n=87).

Parameters	Number (%)
Age (years)	
<50	30 (34.5)
≥50	57 (65.5)
Subtypes of cancer	
TNBC	20 (23.0)
Her2	21 (24.1)
Luminal A	22 (25.3)
Luminal B	24 (27.6)
Tumor size	
<2 cm	23 (26.4)
2-4 cm	58 (66.7)
>4 cm	6 (6.9)
Histological grade	
I	2 (2.4)
II	57 (55.0)
III	17 (15.0)
Unknown	11(27.6)
ER status[a]	
Positive	46 (52.9)
Negative	41 (47.1)
PR status[a]	
Positive	43 (49.4)
Negative	44 (50.6)
Her2 status	
Positive	32 (36.8)
Negative	55 (63.2)
Ki-67(%)	
<14	28 (32.2)
≥14	59 (67.8)

[a]Positive >1%. TNBC, triple negative breast cancer; ER, estrogen receptor; PR, progesterone receptor.

Expression Profiling Interactive Analysis (GEPIA; http://gepia. cancer-pku.cn/index.html).

Statistical analysis. All experiments were independently performed at least three times. The mean ± SD was determined for each group. Statistical analyses were performed using one-way analysis of variance (ANOVA) for multiple group comparisons or Student's t-test for individual comparisons. Multiple comparisons between the groups were performed using the Student-Newman-Keuls method. Statistical significance was considered at $P<0.05$.

Results

SAS reduces breast cancer cell growth. The effects of SAS on breast cancer were investigated. Different human breast cancer cell lines (MDA-MB-231 and T47D, representing TNBC and ER⁺ breast cancer, respectively) were used. Previous studies have reported that higher levels of SAS can reduce glioma cell growth (14). Both breast cancer cell lines were treated with two different concentrations of SAS for 24 h. Microscopic observation revealed that cell growth and viability were significantly inhibited. The two cell lines displayed a significant reduction in cell viability in response to 1.0 and 2.0 mM SAS (Fig. S1). To better understand the effect of SAS in breast cancer cells, the inhibition rate for MDA-MB-231 cells was determined by treating the cells with 1.0 or 2.0 mM SAS at 3, 6, 12 and 24 h. In fact, 2.0 mM SAS induced death in >70% of the breast cancer cells in a time-dependent manner, peaking at 24 h. With an increase in SAS treatment time, the cell growth inhibition rate also increased, and the inhibition rate in the 2.0 mM group was higher than that in the 1.0 mM group (Fig. 1A). Similar results were obtained in T47D cells (Fig. 1B). To confirm the effects of SAS in breast cancer, two other breast cancer lines (BT549 and MCF7, representing TNBC and ER⁺ breast cancer, respectively) were included. The four breast cancer cell lines were treated with different concentrations of SAS for 24 h. The inhibition rates were dependent on the SAS concentration (Fig. 1C). From the trend indicated in the figure, ER⁺ breast cancer cells (T47D and MCF7) were less sensitive to SAS than TNBC cells (MDA-MB-231 and BT549) at the same concentrations. To confirm our hypothesis, the half maximal inhibitory concentration (IC_{50}) of the four cell lines for SAS, was examined. The results revealed that the IC_{50} values of MDA-MB-231 and BT549 cells were significantly lower than those of T47D and MCF7 cells (Fig. 1D). Therefore, SAS reduced the growth of breast cancer cells; however, the sensitivity varied for different breast cancer cells.

Ferroptosis is induced by SAS in breast cancer cells. It was demonstrated that SAS could reduce cell growth, however, whether this effect was due to ferroptosis required more evidence. A large and growing body of literature has demonstrated that xCT and GPX4 play important roles in ferroptosis (15). Previous studies have indicated that inhibition of xCT triggers ferroptosis and that GPX4 plays a role in preventing ferroptosis (5). Traditionally, western blotting has been used to assess the expression of xCT and GPX4. A clear decreasing trend in xCT and GPX4 expression with an increasing concentration of SAS were observed. Similar results were obtained in MDA-MB-231 and T47D cells (Fig. 2A). The accumulation of ROS in cells is a direct cause of ferroptosis (16). Flow cytometry is currently the most popular method for detecting ROS. MDA-MB-231 cells treated with 1.0 or 2.0 mM SAS displayed increased ROS production than untreated and negative control cells (Fig. 2B). Similar results were obtained in T47D cells (Fig. 2C). Detailed flow cytometric data is revealed in Fig. S1.

Many studies have revealed that iron is closely related to oxidative stress. If iron ions cannot bind to proteins or other ligands in an appropriate manner, they can catalyze the formation of metabolically toxic ROS through the H:O: Dependent Fenton reaction. Iron chelators (DFO) and ferroptosis-specific inhibitors (liproxstatin-1) have no significant effects on other forms of cell death (7). Therefore, these reagents can be used to confirm that the death mode caused by SAS is ferroptosis. Liproxstatin-1 prevents ROS accumulation and cell death in
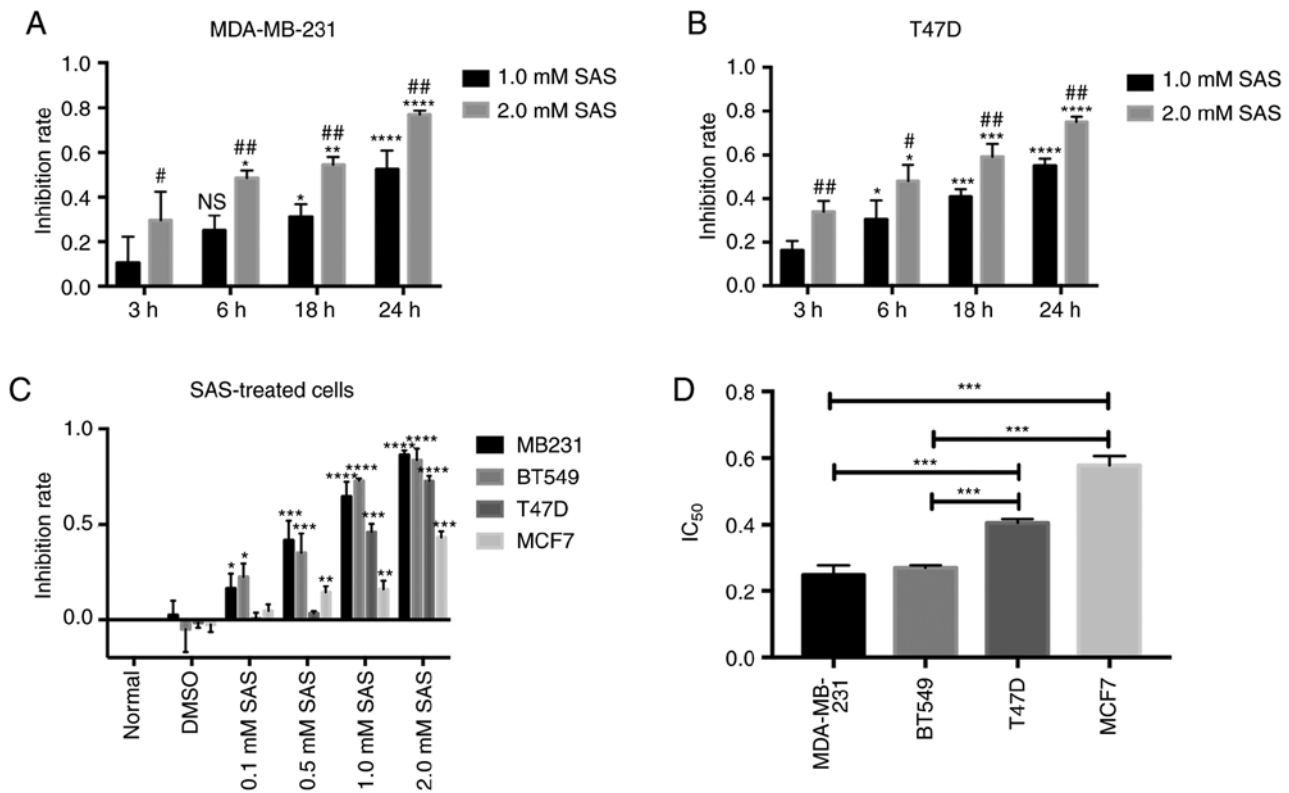
Figure 1. SAS reduces breast cancer cell growth. (A and B) Growth inhibition rates for MDA-MB-231 and T47D cells treated with 1.0 or 2.0 mM SAS at different time-points were detected by CCK-8 assays in at least three independent experiments. Bar graphs represent the mean ± SD. $^*P<0.05$, $^{**}P<0.01$, $^{***}P<0.005$ and $^{****}P<0.001$ compared with the group treated with 1.0 or 2.0 mM SAS for 3 h. $^\#P<0.05$ and $^{\#\#}P<0.01$ compared with the group treated with 1.0 mM SAS for same time. ns, indicates no significant difference. (C) Growth inhibition rates for MDA-MB-231, BT549, MCF7 and T47D cells treated with 0.1, 0.5, 1.0 and 2.0 mM SAS for 24 h were detected by CCK-8 assays in at least three independent experiments. (D) IC$_{50}$ for ER$^-$ cells (MDA-MB-231 and BT549) and ER$^+$ cells (T47D and MCF7) were detected by CCK-8 assays in at least three independent experiments. Bar graphs represent the mean ± SD; $^{***}P<0.005$. SAS, sulfasalazine; ER, estrogen receptor.

cells. Moreover, liproxstatin-1 inhibits ferroptosis induced by ferroptosis-inducing agents (FINs; a series of small molecule inducers, e.g., erastin) *in vitro* (17). Liproxstatin-1 has also been used to determine whether SAS-induced cell death is ferroptosis (18). The results, as revealed in Fig. 2D, indicated that SAS-induced ROS generation can be inhibited by liproxstatin-1 in MDA-MB-231 cells; similar results were obtained in T47D cells (Fig. 2E).

Change in mitochondrial morphology is also a characteristic of ferroptosis (19). Transmission electron microscopy revealed that compared with untreated cells (Fig. 3A), T47D cells treated with 1.0 mM SAS for 24 h had shrunken mitochondria with increased membrane density (Fig. 3B). The white arrow in the figure indicates the mitochondria of T47D cells. This phenomenon was more pronounced in cells treated with 2.0 mM SAS for 24 h (Fig. 3C). Notably, numerous autophagosomes were found in cells treated with 2.0 mM SAS (Fig. 3D), indicating that SAS may induce autophagy. Literature studies have indicated that ferroptosis may be related to autophagy (20). However, further research is required to demonstrate this hypothesis. The same positive result was not obtained in MDA-MB-231 cells. Next, MMP was examined using the probe TMRM, which accumulates in the mitochondria and produces bright red fluorescence in living cells. Confocal microscopy analysis of red fluorescence intensity revealed that compared with untreated cells,

SAS-treated MDA-MB-231 cells displayed a reduction in red fluorescence; similar results were obtained for T47D cells (Fig. 3E). These data indicated that SAS induced mitochondrial depolarization, consistent with the morphological characteristics of ferroptosis observed by transmission electron microscopy. In summary, the mode of death caused by SAS was in fact ferroptosis.

TFRC and DMT1 are activated after the SAS treatment of breast cancer cells. Iron metabolism and lipid peroxidation signaling are increasingly being recognized as central mediators of ferroptosis (21). Fe^{3+} is imported into cells through the membrane protein TFRC and then sequestered in endosomes. In the endosome, Fe^{3+} is reduced to ferrous iron (Fe^{2+}). DMT1, also known as natural resistance-associated macrophage protein 2, belongs to the soluble carrier family member (solute carrier family 11 member 2, SLC11A2) and is a proton-dependent metal ion transporter. DMT1 can mediate transmembrane transport, including Cu^{2+}, Fe^{2+}, Zn^{2+}, and Mn^{2+} ions and is considered to be a transporter of various divalent metal ions in mammalian cells. When the concentration of metal ions in the body changes, DMT1 expression may change accordingly, and it plays an important physiological role in the metabolism and balance of divalent metal ions in cells. The literature indicates that DMT1 mediates the release of Fe^{2+} from the endosome into a labile iron pool in the
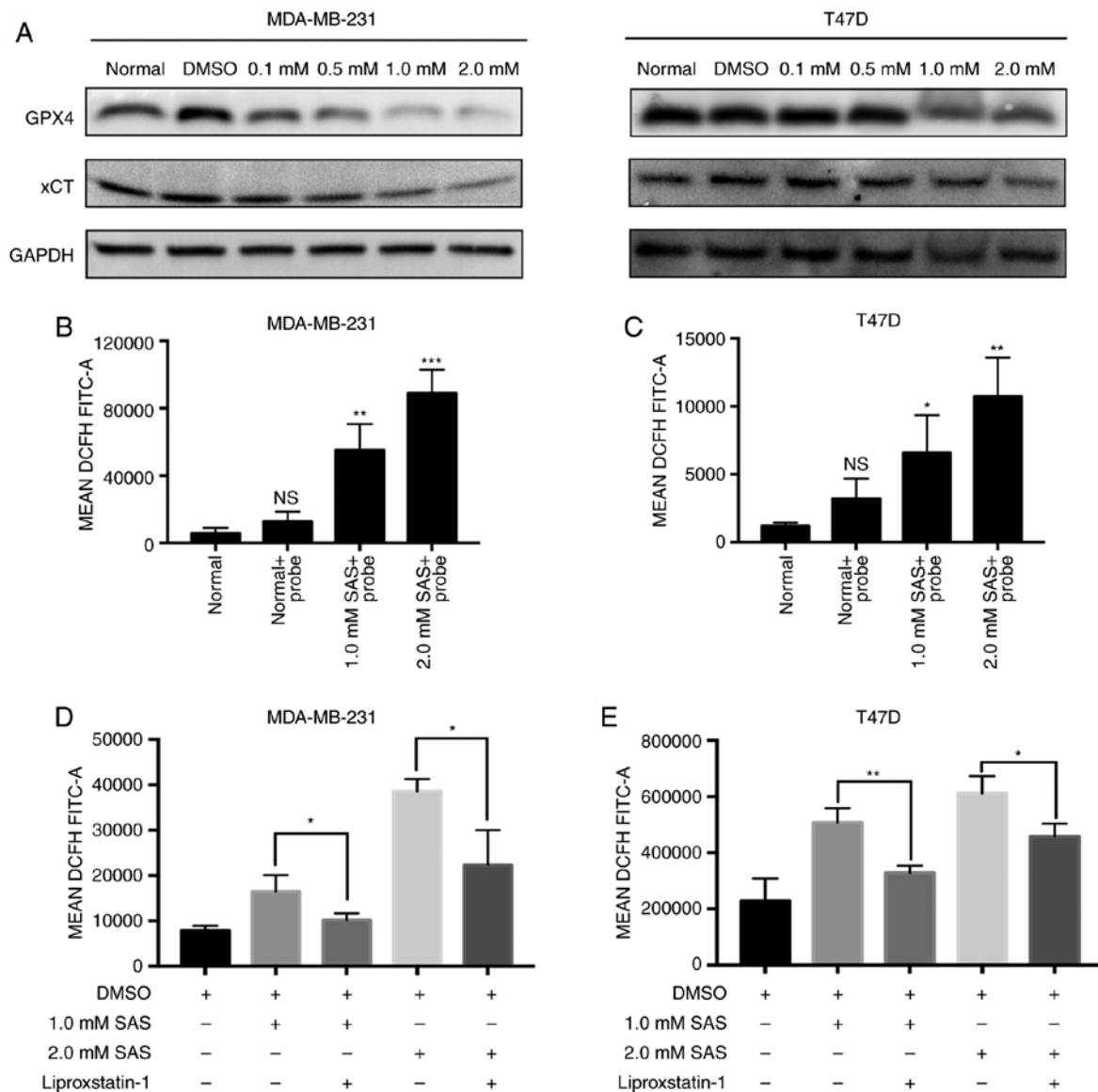
Figure 2. Ferroptosis is induced by SAS in breast cancer cells. (A) Expression of GPX4, xCT and GAPDH in MDA-MB-231 and T47D cells treated with 0.1, 0.5, 1.0 and 2.0 mM SAS for 24 h was detected by western blotting. (B) ROS accumulation in MDA-MB-231 cells without the DCFH-DA probe and treated with 1.0 and 2.0 mM SAS and exposed to the DCFH-DA probe was determined using flow cytometry. Bar graphs represent the mean ± SD. **P<0.01 and ***P<0.005 compared with the normal group. ns, indicates no significant difference. (C) ROS accumulation in T47D cells without the DCFH-DA probe and treated with 1.0 and 2.0 mM SAS and exposed to the DCFH-DA probe was determined using flow cytometry. Bar graphs represent the mean ± SD. *P<0.05 and **P<0.01 compared to normal group. ns, indicates no significant difference. (D) MDA-MB-231 cells were treated with 1.0 or 2.0 mM SAS with or without liproxstatin-1. Flow cytometry was used to detect ROS accumulation in at least three independent experiments. Bar graphs represent the mean ± SD. *P<0.05. (E) T47D cells were treated with 1.0 or 2.0 mM with or without liproxstatin-1. Flow cytometry was used to detect ROS accumulation in at least three independent experiments. Bar graphs represent the mean ± SD. *P<0.05 and **P<0.01. SAS, sulfasalazine; GPX4, glutathione peroxidase 4; ROS, reactive oxygen species; DCFH-DA, 2',7'-dichlorofluorescein diacetate.

cytoplasm (22). Therefore, the accumulation of iron in cells is closely related to TFRC and DMT1. However, the role of SAS in iron metabolic pathways is unknown. To explore the function of SAS in iron metabolic pathways, RT-PCR was used to detect the expression of TFRC and DMT1 in cells treated with different concentrations of SAS. As revealed in Fig. 4A and B, as the SAS concentration increased, the expression of TFRC and DMT1 increased in MDA-MB-231 cells. Consistent with the results in MDA-MB-231 cells, TFRC and DMT1 expression also increased in T47D cells in response to increasing SAS concentrations (Fig. 4C and D), indicating that SAS may activate TFRC and DMT1 to induce ferroptosis.

ER inhibits TFRC expression in breast cancer cells. TFRC is a key factor in iron metabolism, and after determining the role of TFRC in ferroptosis in breast cancer cells, its expression in breast cancer tissues was also investigated. First, TFRC expression was determined in cancer tissues and normal tissues using GEPIA. As revealed in Fig. 5A, TFRC expression in tumor tissues was significantly higher than that in normal tissues. TFRC expression was detected in different breast cancer tissues using immunohistochemistry. Next, bioinformatics was used to analyze TFRC expression in breast cancer subtypes. As revealed in Fig. 5B, TFRC expression in basal (TNBC usually has a basal molecular phenotype) and Her2
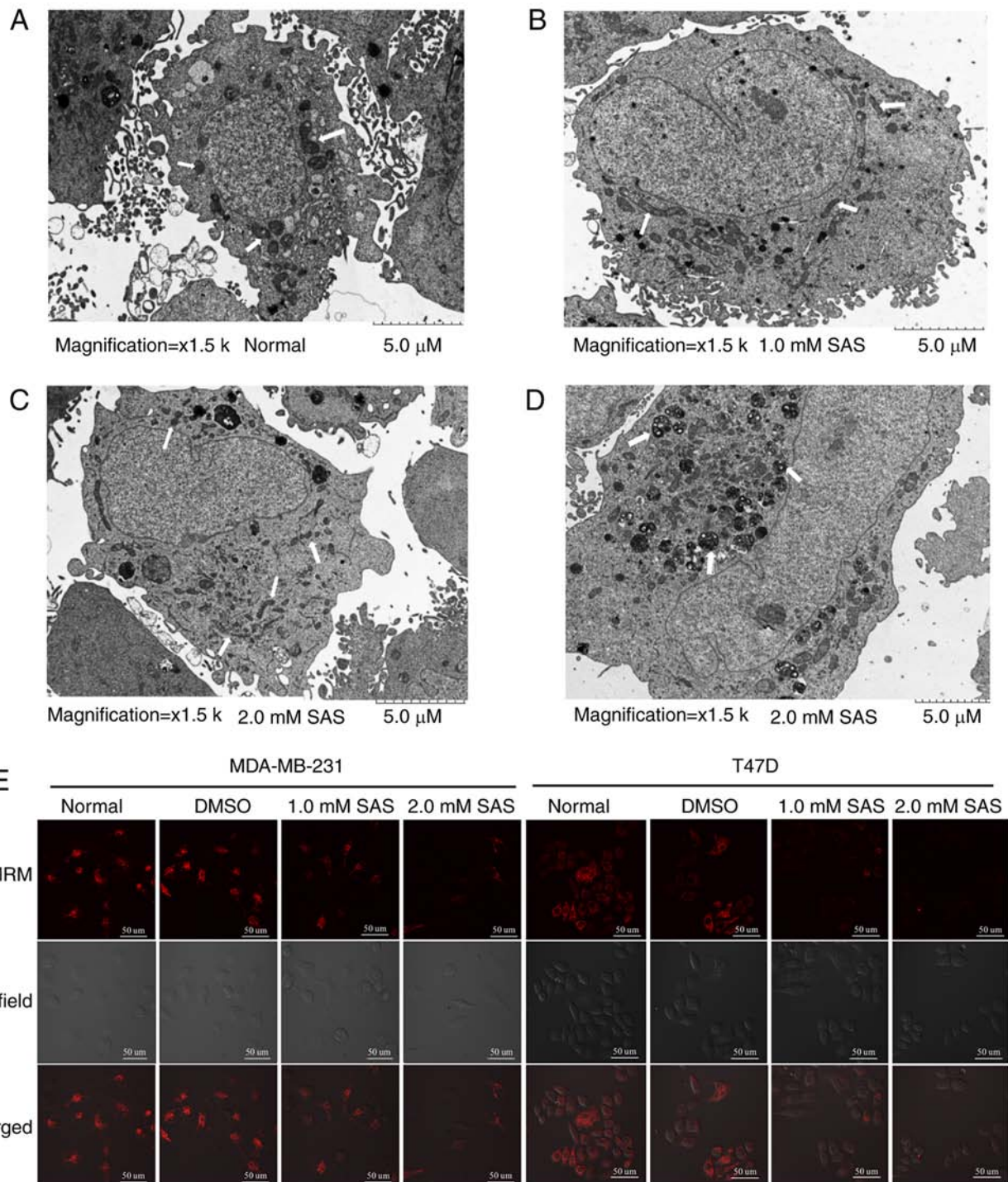
Figure 3. Morphological changes in the mitochondria of breast cancer cells treated with SAS. T47D cells were treated with 1.0 and 2.0 mM SAS for 24 h, and images were captured with a transmission electron microscope. (A) Images of T47D cells without SAS under an electron microscope. The white arrow refers to the mitochondria. (B) Morphological changes in the mitochondria of cells treated with 1.0 mM SAS. The white arrow indicates the mitochondria. (C) T47D cells treated with 2.0 mM SAS observed by transmission electron microscopy. The white arrow indicates the smaller mitochondria. (D) Transmission electron microscopy revealed the presence of many autophagosomes in the cells treated with 2.0 mM SAS. The white arrow indicates the autophagosomes. (E) Representative fluorescence microscopic images of MDA-MB-231 and T47D cells treated with different concentrations of SAS and stained with TMRM. SAS, sulfasalazine; TMRM, tetramethylrhodamine methyl ester.

subtypes was higher than that in luminal and normal subtypes. The expression of ER is negative in TNBC and Her2+ breast cancer. Therefore, the relationship between ER and TFRC was determined. Bioinformatics was used again to analyze the correlation between TFRC and ER. Notably, a negative correlation between TFRC and ER (Fig. 5C) was revealed.

This result may explain why T47D cells are less sensitive than MDA-MB-231 cells to SAS-induced ferroptosis (Fig. 1D). To obtain more convincing results, clinical samples of different tissue types were selected for IHC. The results revealed that TFRC expression was significantly higher in breast cancer tissues of basal and Her2+ cells than in luminal type cancer
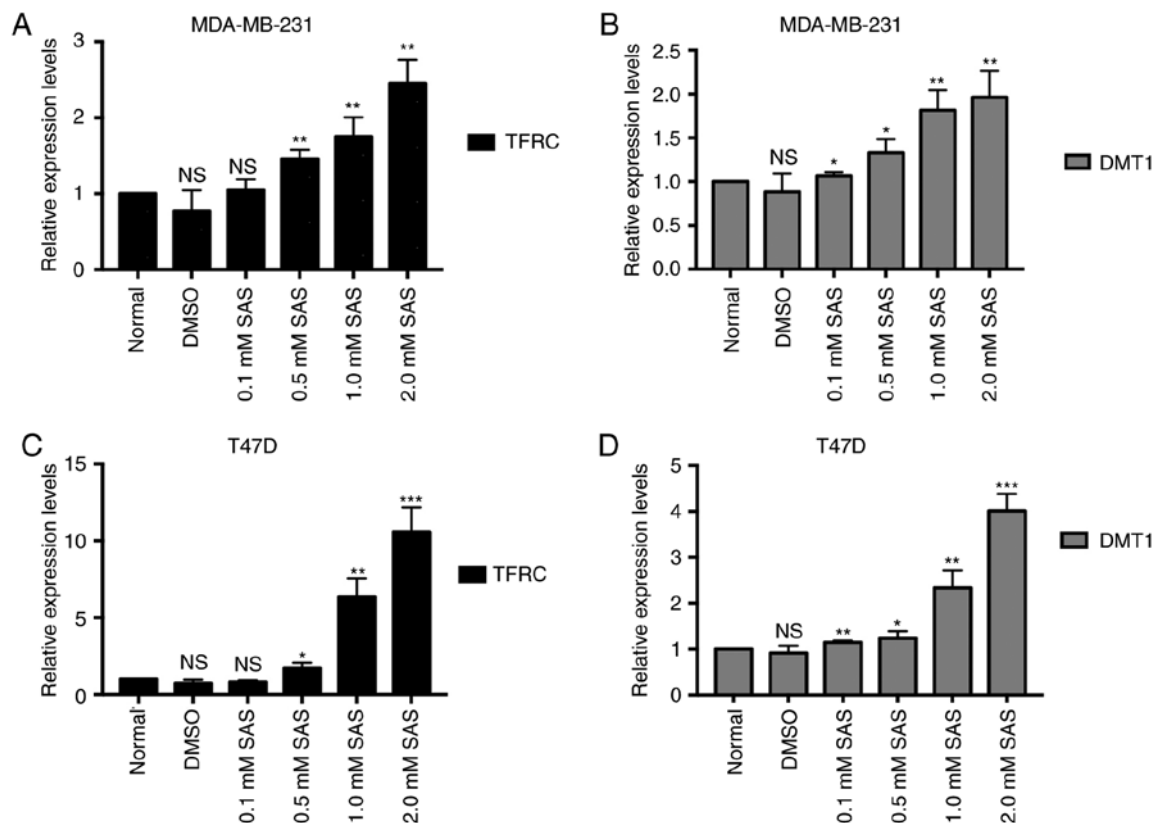
Figure 4. TFRC and DMT1 activation contributes to SAS-induced ferroptosis. (A and B) Expression of TFRC and DMT1 in MDA-MB-231 cells treated with 0.1, 0.5, 1.0 and 2.0 mM SAS for 24 h was detected by RT-PCR from at least three independent experiments using GAPDH as an internal reference. Bar graphs represent the mean ± SD, *P<0.05 and **P<0.01 compared with the normal group. ns, indicates no significant difference. (C and D) T47D cells were treated as aforementioned and detected by RT-PCR from at least three independent experiments using GAPDH as an internal reference. Bar graphs represent the mean ± SD. *P<0.05, **P<0.01 and ***P<0.005 compared with the normal group. ns, indicates no significant difference. TFRC, transferrin receptor; DMT1, divalent metaltransporter 1; SAS, sulfasalazine.

tissues. This finding was consistent with the results of our previous bioinformatics analysis (Fig. 5D). Similar results were obtained in different breast cancer cells. TFRC expression was lower in ER⁺ breast cancer cell lines (T47D and MCF7) than in TNBC cells (BT549 and MB231) (Fig. 5E). Due to the different TFRC expression levels, the sensitivity to SAS-induced ferroptosis varies. The difference in TFRC expression may be due to differences in ER expression in different breast cancer cells. To verify our speculation, siRNAs were used to knockdown ESR1 (the gene encodes the ER) in T47D cells. As revealed in Fig. 5F and H, the expression of ER was successfully knocked down at both the RNA and protein levels. In response to ER knockdown, an increase in TFRC expression (Fig. 5G and H) was observed. These results demonstrated that ER may inhibit TFRC. As revealed in Fig. 1C, MDA-MB-231 and T47D cells had the greatest difference in sensitivity to SAS at concentrations of 0.1 and 0.5 mM. Therefore, these two concentrations were selected for the following experiments. Low concentrations of SAS (0.1 and 0.5 mM) were used to treat ER-knockdown T47D cells. Subsequently, CCK-8 assays were used to assess the SAS-mediated inhibition of T47D cells. The inhibition rate was significantly increased after knocking down ER (Fig. 5I). Collectively, our findings indicated that ER has a protective effect on SAS-induced ferroptosis, and the inhibition of TFRC expression may be one of the underlying mechanisms. To determine TFRC

expression in breast cancer tissues, 87 clinical tissue samples from patients with breast cancer were collected and total RNA was extracted. RT-PCR was used to detect TFRC expression in these different breast cancer tissues. Concurrently, to identify new relationships between TFRC and clinical characteristics, the clinical data was analyzed. As revealed in Fig. 6A, TFRC was expressed at lower levels in ER⁺ breast cancer tissues than in ER⁻ breast cancer tissues, indicating that ER may inhibit TFRC. This result was consistent with our findings in the *in vitro* cell experiments. TFRC expression in tissues representing different breast cancer subtypes was also consistent with TCGA database analysis results. Compared with other subtypes, the Her2 subtype had the highest expression of TFRC (Fig. 6B). Indicative of the relationship between the Her2 gene and TFRC, a high expression of TFRC in Her2⁺ breast cancer tissues (Fig. 6C) was observed. Estrogen is a messenger that must bind to cellular receptors to function. Once combined with estrogen, the ER is activated and transported into the nucleus. After gene transcription leads to PR synthesis, PR synthesis must be achieved by the action of ER synthesis. PR synthesis occurs in conjunction with ER synthesis. Therefore, if the PR is expressed, the ER must also be expressed. Therefore, the expression patterns of the two receptors are similar. The expression of TFRC in PR⁻ breast cancer tissues was higher than that in PR⁺ breast cancer tissues (Fig. 6D). The relationship between TFRC expression and TNM stage, histological
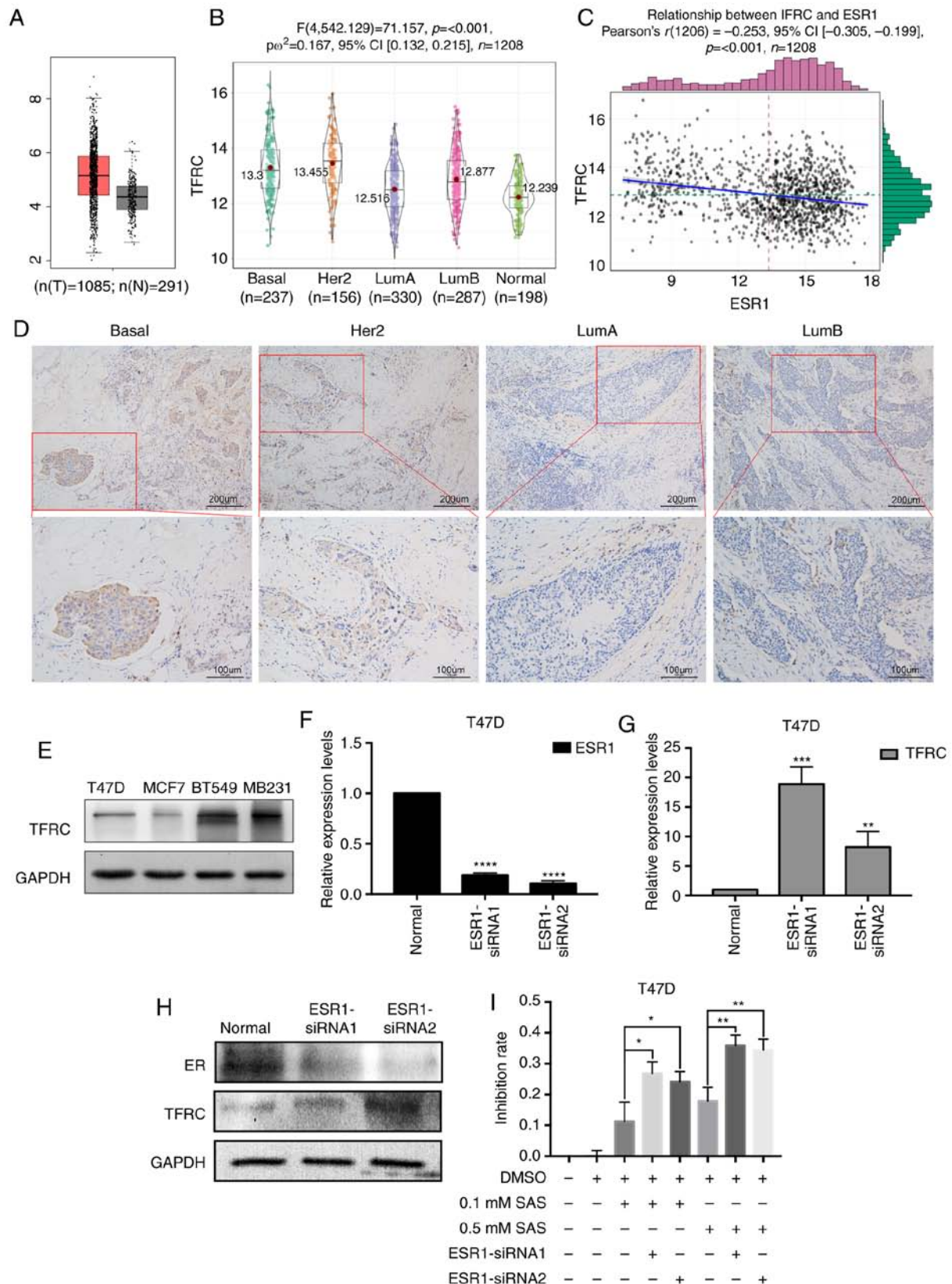
Figure 5. ER inhibits TFRC expression in breast cancer cells. (A) TFRC expression patterns in tumor tissues and normal tissues were determined using GEPIA (http://gepia.cancer-pku.cn/index.html). (B and C) Data for 1,208 breast cancer samples were downloaded from TCGA (https://cancergenome.nih.gov). TFRC expression in different subtypes of breast cancer and the correlation between TFRC and ESR1 were analyzed with 'ggstatspot' (an R language plugin). (D) Different types of breast cancer tissue specimens were collected and organized. Immunohistochemistry was used to detect TFRC expression in tissues. (E) Proteins from different breast cancer cells were extracted, and the expression of TFRC was detected by western blotting. (F and G) T47D cells were transfected with 2 siRNAs against ESR1 for 24 h. Expression of ESR1 and TFRC was determined by RT-PCR. Bar graphs represent the mean ± SD. [**]P<0.01, [***]P<0.005 and [****]P<0.001. (H) T47D cells were transfected with 2 siRNAs against ESR1 for 24 h. Expression of ER and TFRC was determined by western blotting. (I) T47D cells were transfected with 2 siRNAs against ESR1 for 24 h and treated with 0.1 or 0.5 μM SAS for 24 h. Growth inhibition rate was determined using CCK-8 assays in at least three independent experiments. Bar graphs represent the mean ± SD. [*]P<0.05 and [**]P<0.01. ER, estrogen receptor; TFRC, transferrin receptor; GEPIA, Gene Expression Profiling Interactive Analysis; ESR1, estrogen receptor 1.
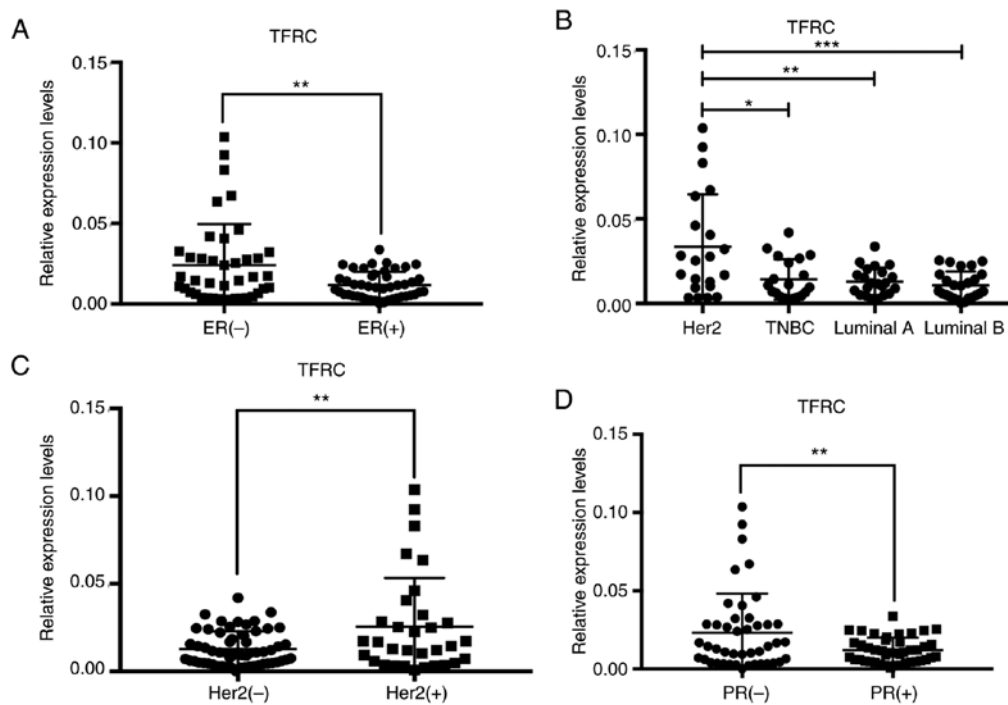
Figure 6. A total of 87 breast cancer tissue samples were collected, and total RNA was extracted. TFRC expression was detected by RT-PCR. (A) TFRC expression in breast cancer tissues with different ER levels. (B) TFRC expression in breast cancer tissues of different molecular types. (C) TFRC expression in breast cancer tissues with different Her2 levels. (D) TFRC expression in breast cancer tissues with different PR levels. *P<0.05, **P<0.01 and ***P<0.005. TFRC, transferrin receptor; PR, progesterone receptor.

grade and Ki-67 expression was also explored, however, no significant associations were revealed (Fig. S1).

Discussion

Research on ferroptosis has been continuing at a steady pace since this phenomenon was discovered in 2012. From numerous previous studies, it is recognized that iron metabolism and lipid peroxidation are two important pathways leading to ferroptosis (7). The inhibition of system x_c^- plays a role during the beginning of lipid peroxidation, which triggers ferroptosis. System x_c^- is a heterodimeric cell surface amino acid antiporter composed of the twelve-pass transmembrane transporter protein SLC7A11(xCT) linked by a disulfide bridge to the single-pass transmembrane regulatory protein SLC3A2 (23). Therefore, it is common to detect the expression of system x_c^- by assessing the level of xCT. System x_c^- imports extracellular cystine into cells in exchange for intracellular glutamate (5,22).

xCT is highly expressed in diverse malignancies, including TNBC and is induced by chemotherapy (24,25). Previous studies have indicated that targeting the novel MUC1-C/xCT pathway could represent a potential therapeutic approach for promoting TNBC cell death (26). A breakthrough study published in 2013 stated that xCT inhibition with the clinically approved anti-inflammatory agent SAS decreases tumor growth, thereby revealing a therapeutic target in breast cancer patients with the poorest prognosis and identifying a lead compound for rapid and effective drug development (25). The study clearly stated that xCT is a compelling therapeutic target for TNBC and that the combination of SAS and carboplatin is very effective for TNBC and may even be recommended for

clinical use. However, the study did not explain the relationship between SAS and ferroptosis or address the role of SAS in other molecular subtypes of breast cancer.

Many small molecules or drugs, such as erastin, SAS, and sorafenib, have been revealed to trigger ferroptosis by inhibiting xCT. Notably, the molecular structures of the three drugs are very similar (15). SAS, a widely used drug for chronic inflammation, can have the same effect as antitumor drugs such as sorafenib, and is therefore of research interest. Inhibition of the NF-κB signaling pathway may be one of the underlying mechanisms (27). Even more notable is the fact that SAS can induce cell death in a variety of malignancies, such as pancreatic cancer (11) and glioma (14). Recently, Tang *et al* reported that cystine deprivation triggered necrosis in TNBC cells (28), and Wang and Yang revealed that ADR increased the expression of SLC7A11 in TNBC, while the inhibition of the SLC7A11 antiporter system sensitized TNBC cells to ADR (29). These results indicated that SLC7A11 is a potential target for the enhancement of the anticancer efficacy of conventional therapies in patients with TNBC. However, these studies are limited to TNBC and SLC7A11 (xCT) and do not address other molecular subtypes of breast cancer or explore iron metabolism pathways.

Iron is essential for the execution of ferroptosis. Both membrane permeable and membrane impermeable iron chelators prevent cells from undergoing ferroptosis, irrespective of whether it is induced by erastin, RSL3 or a physiological stimulus such as a high concentration of extracellular glutamate (30,31). Likewise, ferroptosis induced by erastin or Cys2 deprivation can be prevented by the genetic silencing of the TFRC gene, which encodes the transferrin receptor required

for the uptake of transferrin-iron complexes into cells (32). These results firmly establish the need for iron in ferroptosis. However, how iron promotes ferroptosis inside the cell remains unclear. A recent study revealed that clinically approved SAS enhanced the death of pancreatic cancer cells induced by piperlongumine (PL) and that the combined effects were abrogated by ferroptosis inhibitors and DFO (33). Therefore, it was hypothesized that the activity of SAS is related to the iron metabolic pathway.

In the present study, using microscopy and CCK-8 analysis, it was demonstrated that SAS could inhibit the growth of TNBC cells (MDA-MB-231) and ER$^+$ breast cancer cells (T47D). It was also revealed that these two cell lines had different sensitivities to SAS. However, whether this growth inhibition is due to ferroptosis required more evidence. Western blotting was used to detect the expression of GPX4 and xCT. Flow cytometry was used to determine changes in ROS, and changes in mitochondrial morphology were detected by transmission electron microscopy. Confocal fluorescence microscopy was used to observe the changes in the MMP. By combining the results of these experiments, it was confirmed that SAS in fact triggered ferroptosis in different breast cancer cells. This result was consistent with the findings of previous studies, revealing that SAS-induced ferroptosis is caused by the inhibition of xCT and an increase in the accumulation of ROS. The present research has some limitations, including the lack of evidence from *in vivo* experiments. Several *in vivo* experiments were attempted, however the results were all negative. The primary explanation for this result is that SAS is a drug mainly used for gastrointestinal inflammation, and it is absorbed in the gastrointestinal tract. When SAS reaches the tumor, the drug concentration is very low, and it will not affect tumor growth *in vivo*. A large body of literature was searched and relevant experiments were revealed in a study published in 2013 (25). This study revealed that SAS can reduce the volume of breast tumors *in vivo*, which can be used as a supplement to our research. Iron metabolism, another important pathway for ferroptosis, has not been reported to be affected by SAS. Therefore, a preliminary exploration of the relationship between SAS and iron metabolism was performed. As revealed in Fig. 4, the expression of TFRC and DMT1 increased with increasing concentrations of SAS, indicating that SAS may activate TFRC and DMT1 to induce ferroptosis.

Unlike previous studies, the present study was not limited to TNBC. When the present results were reviewed, an interesting phenomenon was observed. The ER$^+$ breast cancer cell line T47D did not behave the same as the TNBC cell line MDA-MB-231 (Fig. 1C). This finding may be related to differences in the expression of xCT in different cell lines (25). However, the most important difference between T47D and MDA-MB-231 cells was the expression of the ER. To confirm this notable phenomenon, two other breast cancer lines (BT549 and MCF7, representing TNBC and ER$^+$ breast cancer, respectively) were included. Notably, similar results as with MDA-MB-231 and T47D cells were obtained. Therefore, it was hypothesized that ER has a potential inhibitory effect on SAS-induced ferroptosis.

ER was then knocked down in T47D cells with siRNAs and the cells were treated with a low dose of SAS for 24 h,

and the growth inhibition rate in the cells was assessed. Notably, the inhibition rate for T47D cells was increased after ER-specific siRNA transfection. However, it is still unclear how ER functions. Bioinformatics analysis indicated that ER expression may be associated with TFRC expression. After knocking down ER, RT-PCR was used to detect some of the key factors in ferroptosis. Among the many factors, TFRC expression was revealed to be significantly increased (Fig. 5G); the same effect was observed at the protein level (Fig. 5H). Usually, expression in *in vitro* cell experiments may differ from expression in tissues; thus, the expression at the histological level was verified. To this end, 87 clinical tissue samples were collected as well as their related information. It was revealed that TFRC was expressed at lower levels in ER$^+$ breast cancer tissues than in ER$^-$ breast cancer tissues. Similar results were observed for PR$^+$ and PR$^-$ breast cancer tissues. In contrast, TFRC was more highly expressed in Her2$^-$ breast cancer tissues than Her2$^-$ breast cancer tissues. Thus, ER inhibits the expression of TFRC. It is worth mentioning that the presence of SAS does not alter the expression of TFRC in different breast cancer cells. Simply put, the two are not causal. TFRC expression in TNBC and ER$^+$ breast cancer cells does not change due to the presence or absence of SAS. TFRC expression is altered by the different expression levels of ER in different breast cancer cells (TFRC is highly expressed in low-ER TNBC cells and is low in ER$^+$ breast cancer). TFRC expression varies in breast cancer, which in turn produces different sensitivities to SAS in the different breast cancer cells. It is not SAS that changes the expression of TFRC. In conclusion, SAS can trigger ferroptosis in breast cancer cells, especially cells with low ER expression. Therefore, SAS is a potential agent for breast cancer treatment.

The present study still has some limitations. Firstly, due to the characteristics of the mitochondrial membrane potential detection experiment, DAPI could not be used to stain the nucleus. The purpose of our experiment was to detect mitochondrial membrane potential. For the accuracy of the experiment, cell activity should be maintained during the labeling process. Staining of the nucleus of living cells with DAPI was attempted; however, DAPI could penetrate the cell membrane and enter the nucleus. Of note, if the cells were fixed with formaldehyde and the permeability of the cell membrane was increased with some relevant reagents, then DAPI could enter the cells to stain the nucleus. However, this process would kill the cells, and the authenticity of the results could not be guaranteed. For a variety of complex reasons, only a preliminary exploration of the increase in iron metabolism caused by SAS was performed. In a future study, the effects of SAS on iron will be explored, e.g., by detecting changes in the accumulation of iron in cells. Another key issue is where the ER participates in the effects of SAS on TFRC. This question is in fact difficult to answer from our current experimental results since the relationship between the ER and TFRC has not been observed in previous studies. This phenomenon was only revealed; to determine a mechanism, siRNA was used to knock down the ER and detect TFRC expression. The results were confirmed by bioinformatics technology and finally verified by clinical tissue samples. However, the specific mechanisms and

locations of participation are not very clear in the present findings. In our subsequent research, through the analysis of STRING (https://string-db.org), it was revealed that the relationship between ER and TFRC may be through AKT1, SRC, p53 as well as other genes. Therefore, the answer to this question may be addressed in future studies. In addition, a high expression of TFRC in Her2⁺ breast cancer tissue samples was revealed. A study by Miller *et al* revealed that an iron-regulatory gene signature predicted outcomes in breast cancer (34). Therefore, iron metabolism is closely related to the occurrence and development of breast cancer. However, the exact relationship between the Her2 gene and TFRC remains unknown. These issues are worthy of further study. Finally, the present experiments did not use normal breast epithelial cells for comparison for the following reasons. The main purpose of our study was to investigate the role of SAS in breast cancer, rather than the role in normal breast tissue. In addition, TFRC expression in normal tissues and cancer tissues was also compared by bioinformatics in Fig. 5A. Conversely, it is difficult to find a suitable cell line as a representative of the normal epithelium of the breast. It has been reported that MCF10A cells (cells used as normal controls in many studies) are not representative of normal breast cancer cells (35).

In conclusion, the present study proposed for the first time that SAS can induce ferroptosis in breast cancer cells not only by the inhibition of xCT but also by the activation of iron metabolism. Furthermore, the inhibitory effect of ER on TFRC may explain why breast cancer cells with different molecular types have different sensitivities to SAS-induced ferroptosis. The present results further revealed the functions of the ER in the ferroptosis network and indicated SAS as a potential agent for breast cancer treatment.

Acknowledgements

Not applicable.

Funding

Availability of data and materials

The datasets used during the present study are available from the corresponding author upon reasonable request.

Authors' contributions

HY and CY conceived the study, conducted most of the experiments and drafted the manuscript together. LJ, SG, RC, KL, FQ, KT and YF participated in the collection of clinical samples and analyzed the bioinformatics data. FL and SL conducted the statistical analysis of clinical data and analyzed a large amount of experimental data. All the authors read and approved the manuscript and agree to be accountable for all the aspects of the research in ensuring that the accuracy or integrity of any part of the work are appropriately investigated and resolved.

Ethics approval and consent to participate

The First Affiliated Hospital of Chongqing Medical University Ethics Committee reviewed and approved the use of human tissue specimens and all patients provided written informed consent.

Patient consent for publication

Not applicable.

Competing interests

The authors declare that they have no competing interests.

References

1. Torre LA, Bray F, Siegel RL, Ferlay J, Lortet-Tieulent J and Jemal A: Global cancer statistics, 2012. CA Cancer J Clin 65: 87-108, 2015.
2. Weigelt B and Reis-Filho JS: Histological and molecular types of breast cancer: Is there a unifying taxonomy? Nat Rev Clin Oncol 6: 718-730, 2009.
3. Houessinon A, François C, Sauzay C, Louandre C, Mongelard G, Godin C, Bodeau S, Takahashi S, Saidak Z, Gutierrez L, *et al*: Metallothionein-1 as a biomarker of altered redox metabolism in hepatocellular carcinoma cells exposed to sorafenib. Mol Cancer 15: 38, 2016.
4. Ooko E, Saeed ME, Kadioglu O, Sarvi S, Colak M, Elmasaoudi K, Janah R, Greten HJ and Efferth T: Artemisinin derivatives induce iron-dependent cell death (ferroptosis) in tumor cells. Phytomedicine 22: 1045-1054, 2015.
5. Dixon SJ, Lemberg KM, Lamprecht MR, Skouta R, Zaitsev EM, Gleason CE, Patel DN, Bauer AJ, Cantley AM, Yang WS, *et al*: Ferroptosis: An iron-dependent form of nonapoptotic cell death. Cell 149: 1060-1072, 2012.
6. Xie Y, Hou W, Song X, Yu Y, Huang J, Sun X, Kang R and Tang D: Ferroptosis: Process and function. Cell Death Differ 23: 369-379, 2016.
7. Dixon SJ and Stockwell BR: The role of iron and reactive oxygen species in cell death. Nat Chem Biol 10: 9-17, 2014.
8. Lewerenz J, Hewett SJ, Huang Y, Lambros M, Gout PW, Kalivas PW, Massie A, Smolders I, Methner A, Pergande M, *et al*: The cystine/glutamate antiporter system x(c)(-) in health and disease: From molecular mechanisms to novel therapeutic opportunities. Antioxid Redox Signal 18: 522-555, 2013.
9. Gout PW, Buckley AR, Simms CR and Bruchovsky N: Sulfasalazine, a potent suppressor of lymphoma growth by inhibition of the x(c)-cystine transporter: A new action for an old drug. Leukemia 15: 1633-1640, 2001.
10. Dixon SJ, Patel DN, Welsch M, Skouta R, Lee ED, Hayano M, Thomas AG, Gleason CE, Tatonetti NP, Slusher BS and Stockwell BR: Pharmacological inhibition of cystine-glutamate exchange induces endoplasmic reticulum stress and ferroptosis. Elife 3: e02523, 2014.
11. Lo M, Ling V, Low C, Wang YZ and Gout PW: Potential use of the anti-inflammatory drug, sulfasalazine, for targeted therapy of pancreatic cancer. Curr Oncol 17: 9-16, 2010.
12. Basuli D, Tesfay L, Deng Z, Paul B, Yamamoto Y, Ning G, Xian W, McKeon F, Lynch M, Crum CP, *et al*: Iron addiction: A novel therapeutic target in ovarian cancer. Oncogene 36: 4089-4099, 2017.
13. Livak KL and Schmittgen TD: Analysis of relative gene expression data using real-time quantitative PCR and the 2(-Delta Delta C(T)) method. Methods 25: 402-408, 2001.
14. Sehm T, Fan Z, Ghoochani A, Rauh M, Engelhorn T, Minakaki G, Dörfler A, Klucken J, Buchfelder M, Eyüpoglu IY and Savaskan N: Sulfasalazine impacts on ferroptotic cell death and alleviates the tumor microenvironment and glioma-induced brain edema. Oncotarget 7: 36021-36033, 2016.

15. Cao JY and Dixon SJ: Mechanisms of ferroptosis. Cell Mol Life Sci 73: 2195-2209, 2016.
16. NaveenKumar SK, SharathBabu BN, Hemshekhar M, Kemparaju K, Girish KS and Mugesh G: The role of reactive oxygen species and ferroptosis in heme-mediated activation of human platelets. ACS Chem Biol 13: 1996-2002, 2018.
17. Friedmann Angeli JP, Schneider M, Proneth B, Tyurina YY, Tyurin VA, Hammond VJ, Herbach N, Aichler M, Walch A, Eggenhofer E, et al: Inactivation of the ferroptosis regulator Gpx4 triggers acute renal failure in mice. Nat Cell Biol 16: 1180-1191, 2014.
18. Bogacz M and Krauth-Siegel RL: Tryparedoxin peroxidase-deficiency commits trypanosomes to ferroptosis-type cell death. ELife 7: pii: e37503, 2018.
19. Wei G, Sun J, Hou Z, Luan W, Wang S, Cui S, Cheng M and Liu Y: Novel antitumor compound optimized from natural saponin Albiziabioside A induced caspase-dependent apoptosis and ferroptosis as a p53 activator through the mitochondrial pathway. Eur J Med Chem 157: 759-772, 2018.
20. Kang R, Zhu S, Zeh HJ, Klionsky DJ and Tang D: BECN1 is a new driver of ferroptosis. Autophagy 14: 2173-2175, 2018.
21. Torti SV, Manz DH, Paul BT, Blanchette-Farra N and Torti FM: Iron and cancer. Annu Rev Nutr 38: 97-125, 2018.
22. Yanatori I and Kishi F: DMT1 and iron transport. Free Radic Biol Med 133: 55-63, 2018.
23. Sato H, Tamba M, Ishii T and Bannai S: Cloning and expression of a plasma membrane cystine/glutamate exchange transporter composed of two distinct proteins. J Biol Chem 274: 11455-11458, 1999.
24. Lo M, Wang YZ and Gout PW: The x(c)-cystine/glutamate antiporter: A potential target for therapy of cancer and other diseases. J Cell Physiol 215: 593-602, 2008.
25. Timmerman LA, Holton T, Yuneva M, Louie RJ, Padró M, Daemen A, Hu M, Chan DA, Ethier SP, van t Veer LJ, et al: Glutamine sensitivity analysis identifies the xCT antiporter as a common triple-negative breast tumor therapeutic target. Cancer Cell 24: 450-465, 2013.
26. Hasegawa M, Takahashi H, Rajabi H, Alam M, Suzuki Y, Yin L, Tagde A, Maeda T, Hiraki M, Sukhatme VP and Kufe D: Functional interactions of the cystine/glutamate antiporter, CD44v and MUC1-C oncoprotein in triple-negative breast cancer cells. Oncotarget 7: 11756-11769, 2016.
27. Gout PW, Buckley AR, Simms CR and Bruchovsky N: Sulfasalazine, a potent suppressor of lymphoma growth by inhibition of the x(c)-cystine transporter: A new action for an old drug. Leukemia 15: 1633-1640, 2001.
28. Tang X, Ding CK, Wu J, Sjol J, Wardell S, Spasojevic I, George D, McDonnell DP, Hsu DS, Chang JT and Chi JT: Cystine addiction of triple-negative breast cancer associated with EMT augmented death signaling. Oncogene 36: 4235-4242, 2017.
29. Wang F and Yang Y: Retraction Note to: Suppression of the xCT-CD44v antiporter system sensitizes triple-negative breast cancer cells to doxorubicin. Breast Cancer Res Treat 151: 479, 2015.
30. Yang WS, SriRamaratnam R, Welsch ME, Shimada K, Skouta R, Viswanathan VS, Cheah JH, Clemons PA, Shamji AF, Clish CB, et al: Regulation of ferroptotic cancer cell death by GPX4. Cell 156: 317-331, 2014.
31. Yang WS and Stockwell BR: Synthetic lethal screening identifies compounds activating iron-dependent, nonapoptotic cell death in oncogenic-RAS-harboring cancer cells. Chem Biol 15: 234-245, 2008.
32. Gao M, Monian P, Quadri N, Ramasamy R and Jiang X: Glutaminolysis and transferrin regulate ferroptosis. Mol Cell 59: 298-308, 2015.
33. Yamaguchi Y, Kasukabe T and Kumakura S: Piperlongumine rapidly induces the death of human pancreatic cancer cells mainly through the induction of ferroptosis. Int J Oncol 52: 1011-1022, 2018.
34. Miller LD, Coffman LG, Chou JW, Black MA, Bergh J, D'Agostino R Jr, Torti SV and Torti FM: An iron regulatory gene signature predicts outcome in breast cancer. Cancer Res 71: 6728-6737, 2011.
35. Qu Y, Han B, Yu Y, Yao W, Bose S, Karlan BY, Giuliano AE and Cui X: Evaluation of MCF10A as a reliable model for normal human mammary epithelial cells. PLoS One 10: e0131285, 2015.